J Appl Electrochem (2014) 44:1093–1105
DOI 10.1007/s10800-014-0718-7

RESEARCH ARTICLE

Influence of buffering on the spontaneous deposition of cerium conversion coatings for corrosion protection of AA2024-T3 aluminum alloy

Stephan V. Kozhukharov · Olaia F. Acuña · Maria. S. Machkova · Vladimir S. Kozhukharov

Received: 5 February 2014 / Accepted: 14 July 2014 / Published online: 17 August 2014

Abstract Cerium-based conversion coatings were spontaneously deposited on AA2024-T3 alloy at 60 °C using buffered and non-buffered $CeCl_3$ solutions in the presence of H_2O_2. Malonic acid or amino-acetic acid (glycine) was used as buffering additives. The deposition process and the properties of the coatings obtained were followed by linear voltammetry and electrochemical impedance spectroscopy. The surface morphology was studied by scanning electron microscopy. It was found that buffering complicates the conversion process and hampers the deposition rate. The coatings deposited using buffered baths had lower barrier ability and corrosion durability in 3.5 % NaCl corrosive medium compared to those deposited in the absence of buffers.

Keywords AA2024-T3 alloy · Cerium conversion coatings · Corrosion protection · Electrochemical tests · Surface morphology

1 Introduction

Aluminum alloys are rated second after various steels when used for household and industrial applications. This is due to their excellent strength parameters, low relative weight, and relatively acceptable price. Besides, 70 % of the airplanes are made using aluminum alloys [1]. The latter find also wide application in shipbuilding, automotive, and aerospace industries. The major disadvantages observed refer to their susceptibility to corrosion. It is attributed to the presence of Cu, Mg, Fe, Mn, Si, etc., forming intermetallic phases of various compositions during the aging and the hot rolling finishing stages of the production process [2]. Being in the form of individual particles, these phases are dispersed in the aluminum matrix and become centers of initiation and proliferation of local corrosion at the sites of contact of the alloys with the aggressive corrosive media containing chlorine ions [3–5]. That is why the aluminum alloys application is practically impossible without any corrosion protection. One of the most efficient methods used for more than 50 years refers to the metallic surface modification by deposition of chromate conversion coatings [6, 7]. The latter are not finishing but provide improved adhesion of the paint layers required. Furthermore, the chromate conversion coatings provide active corrosion protection characterized by self-healing of the coating upon its chemical or mechanical damaging [8]. However, the chromium containing coatings are toxic and carcinogenic because of the Cr(VI) presence and which is why they are prohibited in EU [9] and the USA [10, 11].

A great number of organic and inorganic compounds have been examined as environmentally acceptable alternative to chromates. The compounds of the lanthanides are found promising in this respect [12]. Besides, some of these elements are abundant in nature and pose no risk to human health [13].

The pioneer investigations on the applications of lanthanide compounds as inhibitors of aluminum corrosion were carried out by Hinton et al. [14–17]. They found that $CeCl_3$ can protect AA7075 alloy against its uniform and pitting corrosion. The numerous investigations which followed showed that cerium was the most efficient corrosion

S. V. Kozhukharov (✉) · Maria. S. Machkova · V. S. Kozhukharov
University of Chemical Technology and Metallurgy, 8 "Kl. Okhridsky" blvd., 1756 Sofia, Bulgaria
e-mail: stephko1980@abv.bg

O. F. Acuña
University of Vigo, Lagoas, Marcosende, 36310 Vigo, Spain

Table 1 Composition of the AA2024-T3 alloy

Element	Cu	Mg	Mn	Fe	Si	Cr	Zn	Ti	Al
$\%_{weight}$	4.69	1.47	0.64	0.28	0.17	0.02	0.09	0.02	Balance

inhibitor among the lanthanides [18]. The cerium compounds were introduced to the corrosive medium either directly [19–23] or through hybrid [24–27] or conversion coatings [28–32]. Various techniques were applied in the latter case. The deposition was initially performed by dip-coating of aluminum alloy specimens in neutral solutions of simple cerium salts at room temperature. The earliest experiments of the kind were run by Hinton who found that at least 90 h were required for the formation of a cerium conversion film covering the entire sample surface [16]. This prolonged treatment turned out to be commercially unattractive. The temperature increases to 43 °C and peroxide introduction to the deposition solution [17] decreased the deposition time to 10 min.

Cerium conversion coatings have complex composition comprising oxides/hydroxides of Al, Ce(III), and Ce(IV) [33]. It is shown [34] that these coatings have a heterogeneous double-layered structure in case of AA2024 alloy, due to the different mechanism of their formation on the alloy matrix and on the active cathodic and anodic zones on the surface.

The deposition of cerium conversion coatings from peroxide containing solutions is accompanied by alkalization because of peroxide reduction generating OH^- ions and Ce(III) ions oxidation leading to $Ce(OH)_4$ formation. The latter precipitates because of the extremely low value of its solubility product [35] and hence compromises the bath used. There are studies on the deposition of cerium conversion coatings from non-buffered Ce-solutions, but only one reports data connected with buffered solutions application [33]. There, acetic and malonic acids are used as buffering agents. It is found that the bath is stabilized, but the effect on the kinetics of the deposition process and the properties of the coatings obtained remains unclear.

The present communication is aiming to provide further information in this aspect. It reports data on the properties of cerium conversion coatings deposited on AA2024-T3 in buffered and non-buffered solutions of $CeCl_3$ in the presence of H_2O_2.

2 Experimental

2.1 Alloy composition

Table 1 presents the composition of the alloy used. It is a product of Southwest Aluminum Co. Ltd., (China).

2.2 Preliminary treatment of the alloy samples

The pre-treatment applied is very important for the formation and the properties of the coatings considered [36]. Some authors [37, 38] prefer mechanical grinding; others apply chemical superficial modification [8, 29, 36]. These procedures predetermine the metallic surface roughness, the thickness of the superficial oxide layer, as well as the chemical composition of the alloy surface due to the selective dissolution of some of its components. Both preliminary procedures were applied under the following conditions.

2.2.1 Mechanical grinding

Alloy panels sized 25 × 25 × 2 mm were ground with SiC emery paper with successive decrement grit size of 280, 500, 800, 1,000, and 1,200. The specimens were cleaned and degreased for 5 min at room temperature in alcohol/ether mixtures of 1:1 v/v. Prior to the immersion to the bath, the samples were washed with tap and distilled water.

2.2.2 Alkaline etching

This is the most frequently used pre-treatment procedure, because it is the cheapest one and does not require preliminary degreasing. It required etching of the samples through immersion in NaOH solution (50 g L^{-1}) at 50 °C for 90 s, vigorous rinsing with tap-water for at least 1 min and then washing with distilled water. An additional pre-treatment step was introduced because of the formation of a black smut layer composed of the oxides of the heavy metal alloying additives. It required immersion in diluted HNO_3 (1:1 v/v) for 10 min at room temperature to be followed by vigorous rinsing with tap and distilled water.

2.3 Conversion baths and coating deposition regime

Conversion baths of three different compositions were used. The latter are presented in Table 2.

2.4 Surface morphology and coating composition

The optical remission ability of selected specimens was determined in the frame of the visible spectrum with wavelength range from 400 to 700 nm by Lovibond RT

Table 2 Composition of the baths and regime of deposition of the Cerium conversion coatings

Components	Non-buffered bath	Buffered baths	
		Malonic bath	Glycine bath
Solvent	Dist. water	0.1 M Malonic acid	Glycine buffer[a]
$CeCl_3 7H_2O$, M	0.05	0.05	0.05
30 % H_2O_2, mL L^{-1}	12.5	12.5	12.5
Molar ratio, $n_{H_2O_2}:n_{Ce}$	2:1	2:1	2:1
Initial pH value[b]	2.15	2.15	2.15
Temperature, °C	60	60	60
Deposition duration, min	5; 10; 15	5; 10; 15	5; 10; 15

[a] Original glycine buffer, obtained by mixing of two initial solutions: solution of 0.1 M HCl (solution 1) and solution of 7.5 g L^{-1} amino acid (glycine) + 5.85 g L^{-1} NaCl (solution 2) [39]. Regarding the relation of the volumes of both solutions, the pH of the medium could be changed from 1.1 to 3.5

[b] The initial pH value of the solution was reached by addition of HCl

Colour, produced by Tintometer Ltd. (UK). SEM images at different magnifications were recorded using a scanning electron microscope (TESCAN, SEM/FIB LYRA I XMU).

2.5 Barrier properties and corrosion durability

These properties were studied by linear voltammetry (LVA) and electrochemical impedance spectroscopy (EIS). The measurements were performed in a three-electrode electrochemical cell of a volume of 100 mL. Circular-shaped zones on the samples' surface of an exposed area of 2 cm^2 were used as working electrodes. A platinum mesh [40] and Ag–AgCl/3 M KCl (Metrohm, model 6.0733.100) were used as a counter and reference electrode, correspondingly. An aqueous solution (3.5 %) of NaCl was used as a model corrosive medium. The electrochemical cell used was enclosed in a Faraday cage. All experiments were performed at room temperature 24 h after the cell assembling. The latter condition was required to provide a stable open circuit potential (OCP). Then LVA was applied within a narrow potential range around OCP (OCP ± 0.030 V). The scan rate used was of 0.5 mV s^{-1}. The R_p values reported are the average of the closest results. The corresponding electrochemical impedance spectra were recorded in the frequency range from 10^5 to 10^{-2} Hz at 7 frequencies per decade and 20 mV amplitude of the AC potential, in respect of OCP. The impedance measurements were followed by acquisition of cathodic polarization curves in a wide potential interval—from OCP +0.030 V to OCP −0.600 V, at 1.0 mV s^{-1}. All electrochemical measurements were repeated with at least 3 times on a new sample each time.

3 Results and discussion

3.1 Coating deposition from buffered and non-buffered solutions

The spontaneous deposition of cerium conversion coatings is a complex process depending on the preliminary treatment of the substrates, the type and the concentration of the cerium salt used, H_2O_2 concentration, pH of the conversion bath, the presence of buffers, deposition temperature, and time.

Some basic criteria are considered adjusting the bath compositions and the deposition regime (Table 2): (1) the coatings obtained have to be gold-like, uniform, smooth, and of good adhesion to the substrate; (2) the electrolyte used has to remain colorless and transparent; (3) multiple depositions are to be carried out without any additional modification; (4) the deposition process has to be accelerated. The content of $CeCl_3$ and H_2O_2 as well as all other parameters (initial pH value, temperature and deposition time) are kept constant aiming to outline the effect of the buffering additives.

The deposition temperature pointed out in Table 2 seems relatively high when compared to most of the literature values. However, it proved to be an acceptable trade-off. It is so because the deposition process is rather slow at lower temperatures (of the order of 80–90 min); the deposition time is decreased to about 30–40 min at 35 °C, while the coatings become visible within the first 1–2 min in case of the alkaline-etched specimens at 60 °C. It is worth adding that the higher temperatures improve the coating adhesion. But the further temperature increase accelerates peroxide decomposition. Hence, H_2O_2 content adjustment is required after the 3rd or the 4th deposition run. This adjustment is compensated as the adhesion of the coating is improved. It is found that CeCC deposition following immediately H_2O_2 addition does not produce coatings of satisfactory quality. This experimental finding verifies the assumption of Scholes et al. [41] that the deposition of cerium conversion coatings proceeds through a slow intermediate stage of direct interaction of Ce^{3+} ions and H_2O_2 via the formation of complex $Ce(H_2O_2)^{3+}$ species. This reaction takes place in correspondence with

$$Ce^{3+}_{(aq)} + H_2O_{2(aq)} \rightarrow Ce(H_2O_2)^{3+}_{(aq)} \quad (1)$$

The intermediate stage pointed above imposes the necessity of bath aging. The results obtained show that

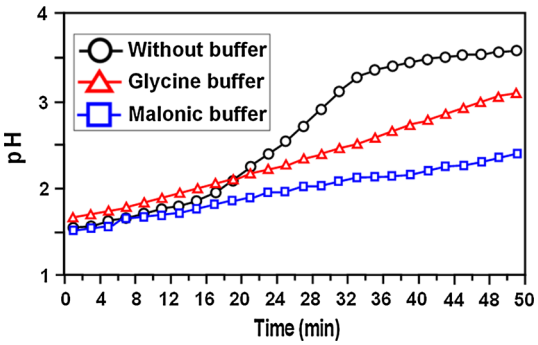

Fig. 1 Evolution of pH of the conversion bath during coating deposition on alkaline-etched AA2024 substrates

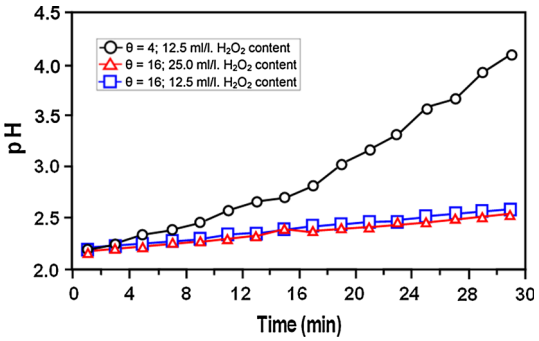

Fig. 2 Evolution of pH of the conversion bath during coating deposition in the presence of malonic buffer at different values of θ and H_2O_2 content

gold-yellow, uniform coatings can be obtained on a second substrate using the same bath with no additional pH and the H_2O_2 content adjustment. This leads to the assumption that, following the first deposition, Al-ions accumulate in the bulk of the solution. Thus, they contribute to the deposition of mixtures of Ce–Al-oxides/hydroxides [34].

The efficiency of the buffers used is illustrated by the "kinetic" curves shown in Fig. 1.

Figure 1 shows that pH of the non-buffered bath in y-axis rises steeply providing conditions for oxidation of Ce(III) to Ce(IV) in the bulk of the solution and for precipitation of Ce(IV) ions in the form of $Ce(OH)_4$. No such pH increase is observed in the presence of a buffer. The oxidation of Ce(III) to Ce(IV) is hampered at low pH values. The use of malonic acid as a buffering agent is not appropriate because of the low pH values reached and the reducing effect observed. An analytical method for quantitative determination of malonic acid by titration with solution of Ce(IV) ions is described in the literature [42]. This method is based on the following reaction:

$$CH_2(COOH)_2 + 6Ce(IV) + 2H_2O \rightarrow HCOOH + 6Ce(III) + 2CO_2 + 3H_2 \quad (2)$$

In malonic acid, buffered solutions complicated redox interactions with the participation of H_2O_2, Ce(III)/Ce(IV), and the malonic acid. It is difficult to present a comprehensive picture of these interactions and the changes that they bring about in the course of the conversion process.

The present investigation shows as well that there is another important parameter related to CeCC deposition. It refers to the ratio of the bath volume V and the total surface area S of the immersed specimens. It represents the bulk loading θ of the electrolyte per unit surface area of the sample and can be designated as "Load per Volume" (LPV). It is found that it affects significantly the conversion process, and hence, the quality of the coatings obtained. This parameter determines the consumption rate of the cerium compound from the electrolyte during the deposition process. Thus, relatively high LPV values correspond to more intensive changes in the electrolyte composition.

$$\theta = V/S \quad (2)$$

The curves in Fig. 1 are obtained using a bath of a volume of 200 mL in which a sample of 12.5 cm^2 surface area is immersed. In this case, $\theta = 16$ cm. These curves are expected to have different profiles and different relative positions at other bulk loadings (i.e., other LPV values). Thus, these curves will be steeper at low θ values because of the solution alkalization. This can be seen in Fig. 2 which illustrates the superimposition of pH/t curves obtained in a bath containing malonic buffer.

Figure 2 shows clearly that low bulk loadings cause a sharp rise of pH/t curves resulting in bath precipitation regardless of the buffering. All differences in the buffered and non-buffered baths behavior reported in the present communication refer to deposition of more than 10 min at 60 °C. The effects observed become indistinguishable when the deposition is performed at room temperature for time less than that mentioned above.

The solution buffering has a beneficial effect in respect to the bath stability, because it prevents the quick increase of pH followed by precipitation phenomena. However, the buffering may have a negative effect on the coatings quality. The results observed in the presence of a malonic buffer and high bulk loading support this suggestion. This is demonstrated by the kinetic curves presented in Fig. 2. The effect considered becomes remarkably evident at high θ values for baths buffered with malonic acid. Dark purple deposits of very poor adhesion are obtained in this case.

Figure 3 represents the optical spectra of coatings deposited from non-buffered bath and a bath with malonic acid buffer. This figure shows the remarkable differences in the optical remission values of the respective coatings. The coating deposited from non-buffered bath reveals a

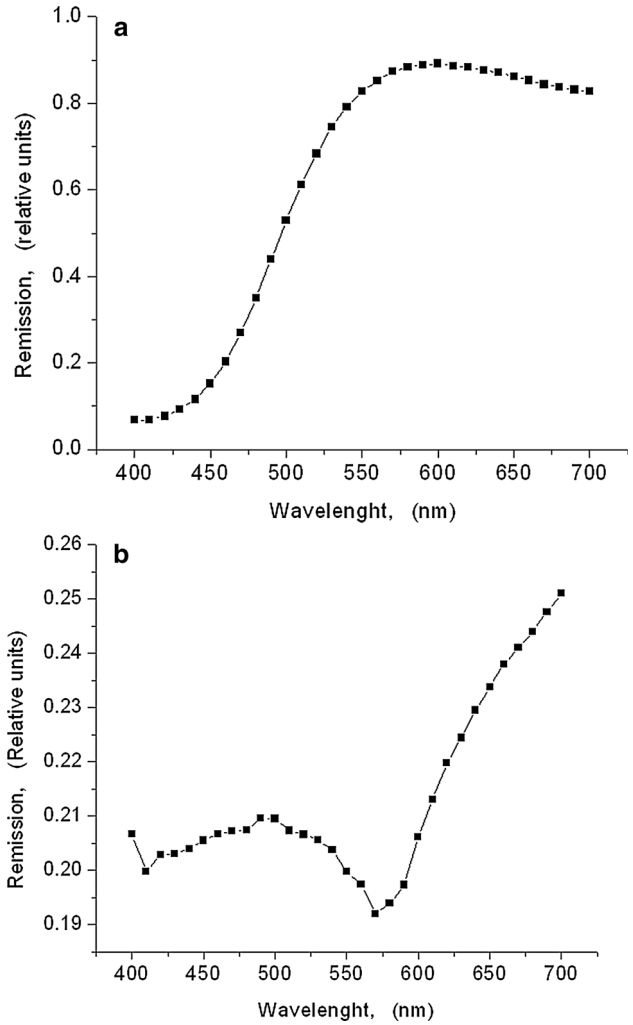

Fig. 3 Optical spectra of coatings deposited from non-buffered bath (**a**), and a bath with malonic acid buffer (**b**)

maximum in the range of 600 nm, corresponding to yellow-greenish color, whereas CeCC obtained from the malonic acid containing bath has two maxima, a smaller one at 500 nm, and much bigger one at the red domain of the visible spectrum (i.e., at 700 nm). This difference in the colors of the specimens is a result of the variations in their composition. It can be suggested that the color of coating obtained from the buffered bath is probably due to the presence cerium hydrides [43] which possess a blue color [44].

The CECCs obtained from glycine buffered conversion bath did not reveal any presence of purple shade, because this buffer does not maintain as low pH value as does the malonic acid. Consequently, the glycine buffer does not suppress the formation of Ce-oxides/hydroxides.

All results discussed above lead to the conclusion that each buffer requires a specific composition of the bath. But the development of bath compositions required by the buffer used is a task beyond the scope of the present work.

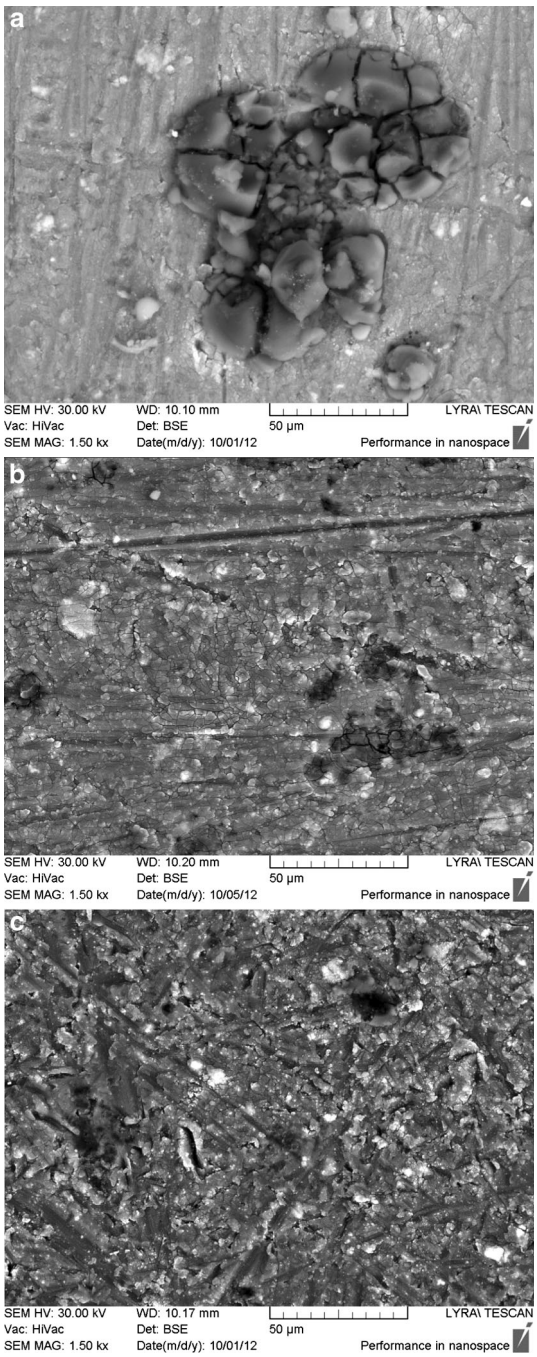

Fig. 4 Superficial SEM images of three specimens after mechanical grinding and subsequent CeCC for 10 min at 60 °C in presence of no buffer (**a**), glycine buffer (**b**) and malonic acid buffer (**c**)

3.2 Surface morphology

As pointed above, the preliminary treatment has a tremendous influence on the deposition process and the properties of the coatings obtained. The pre-treatment induces changes in the superficial oxide layer and the surface roughness. Besides, the etching procedures lead also to a modification of the alloy chemical composition.

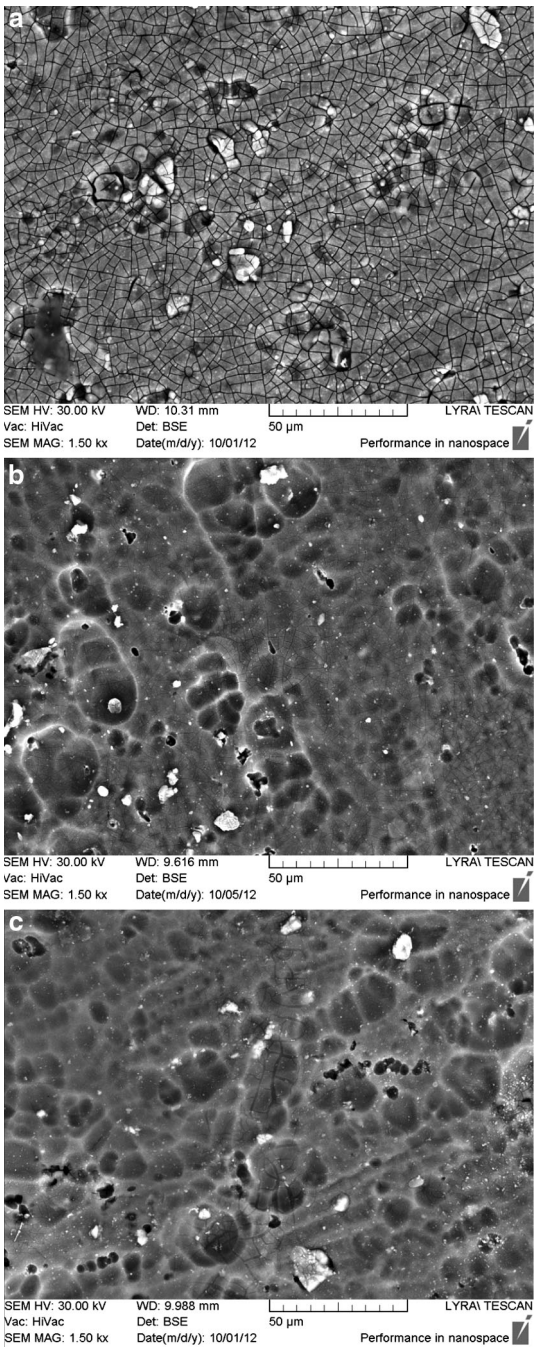

Fig. 5 SEM images of CeCC deposited for 10 min at 60 °C in the absence of a buffer (**a**) and in the presence of glycine (**b**) and malonic acid buffer (**c**) on alkaline-etched substrates

3.2.1 *Mechanically pre-treated specimens*

In order to determine the influence of buffering in the Ce-conversion bath, samples subjected to the same preliminary treatment but immersed in different deposition baths (e.g., without buffer, with glycine or malonic buffer) are compared. Figure 4 shows the SEM images of three samples after identical mechanical preliminary treatment, but

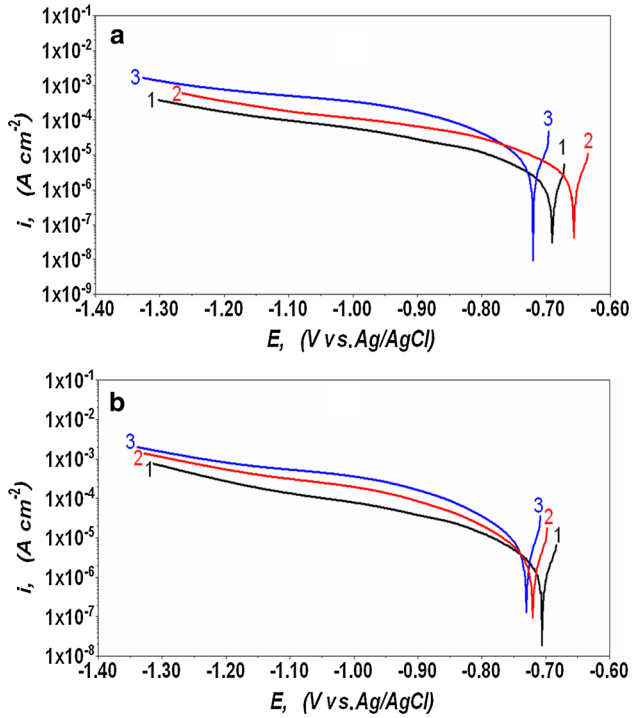

Fig. 6 Cathodic polarization curves of CeCC deposited in baths with no buffer (*1*) and in presence of glycine (*2*) and malonic acid (*3*) buffer on (**a**) mechanically ground (**a**), and alkaline-etched (**b**) alloy samples

submitted to deposition in solutions of no buffer (a) and in solutions containing glycine (b) and malonic (c) buffer.

The micrographs in Fig. 4 reveal apparent differences between the coatings deposited in the absence and in the presence of buffer. Rough areas of heavily cracked thicker deposits are observed in the former case. The clearly visible ruptures in these zones are formed as a result of shrinkage of the coatings when dried. The depositions observed refer to the cathodic areas on the samples' surface abundant in OH^- ions. The latter interact with Ce-ions in the solution to form Ce-hydroxides [45].

The coatings prepared in the presence of a buffer look more uniform because the buffers do not provide formation of local zones of high pH as already discussed. Nevertheless, these coatings have another defect manifested by dark concavities in the SEM images. The number of these craters is greater for the coating deposited in the malonic bath. These defects may result because of incomplete coating deposition which in turn is determined by the lower deposition rate.

3.2.2 *Alkaline-etched specimens*

Figure 5 shows three samples coated at 60 °C for 10 min in Ce-conversion baths. Alkaline etching was the preliminary treatment used.

Table 3 Values of the polarization resistance R_p/kΩ cm^{-2} of CeCC, deposited from buffered and non-buffered baths on mechanically grinded and alkaline-etched specimens

Conversion bath	Preliminary treatment	
	Mechanical	Alkaline
Non-buffered	8.95	8.52
Malonic buffer	2.35	2.33
Glycine buffer	4.28	4.19

All images feature clearly visible wide and shallow concavities in the coatings. They originate from concavities on the substrate surface resulting from the alkaline etching [46, 47]. The coating deposited in the buffer absence has a heavily cracked structure, whereas no visible cracks are observed on the surface of the other two specimens examined.

The cracks in the coating obtained in a buffer-free solution (Fig. 5a) are probably due to the greater thickness of this coating. This coating shrinks in volume and thus suffers much stronger mechanical stress than the other two coatings (Fig. 5b, c) in the course of the subsequent drying process. In fact, all coatings look ruptured at higher magnification (e.g., 10,000 times). This is not shown in the figures discussed.

3.3 Polarization measurements

Figure 6 shows cathodic polarization curves of Ce-conversion coatings deposited on mechanically ground and alkaline-etched specimens of the alloy.

The coatings barrier ability can be assessed qualitatively by comparing the current densities of the curves discussed at definite potentials. It is seen that the coatings deposited in non-buffered baths have the lowest current density and the highest barrier ability. The lowest barrier ability is found for the coatings deposited in the bath containing a malonic buffer.

The polarization measurements provide the determination of the values of the polarization resistance, R_p. The latter is a quantitative measure of the coatings barrier ability. Table 3 summarizes R_p values referring to CeCC deposited in different baths on specimens subjected to different preliminary treatments.

The data in the table show that bath buffering decreases the polarization resistance of the coatings. This results not because of differences in coating structure or composition but is rather a consequence of its lower thickness. The buffering agent maintains low pH values and thus decreases the deposition rate. The process is further retarded by the reducing activity of the buffers which hinder the oxidation of Ce(III) ions to Ce(IV). The glycine bath, proposed in the present work, allows deposition of coatings of R_p values twice higher than that reported [33] for the malonic bath.

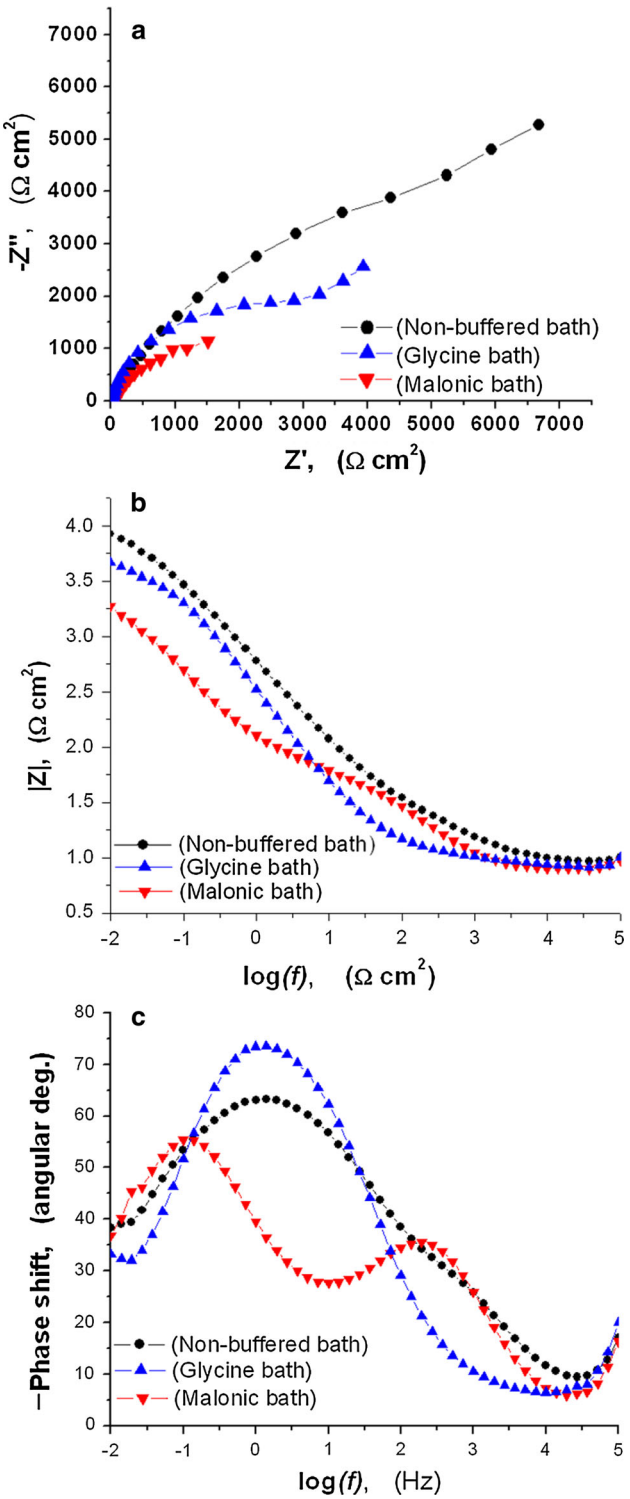

Fig. 7 Impedance spectra, in Nyquist (**a**) and Bode (**b**) plots of CeCC deposited in different baths on mechanically ground AA2024 samples after 24 h of exposure to 3.5 % NaCl solution

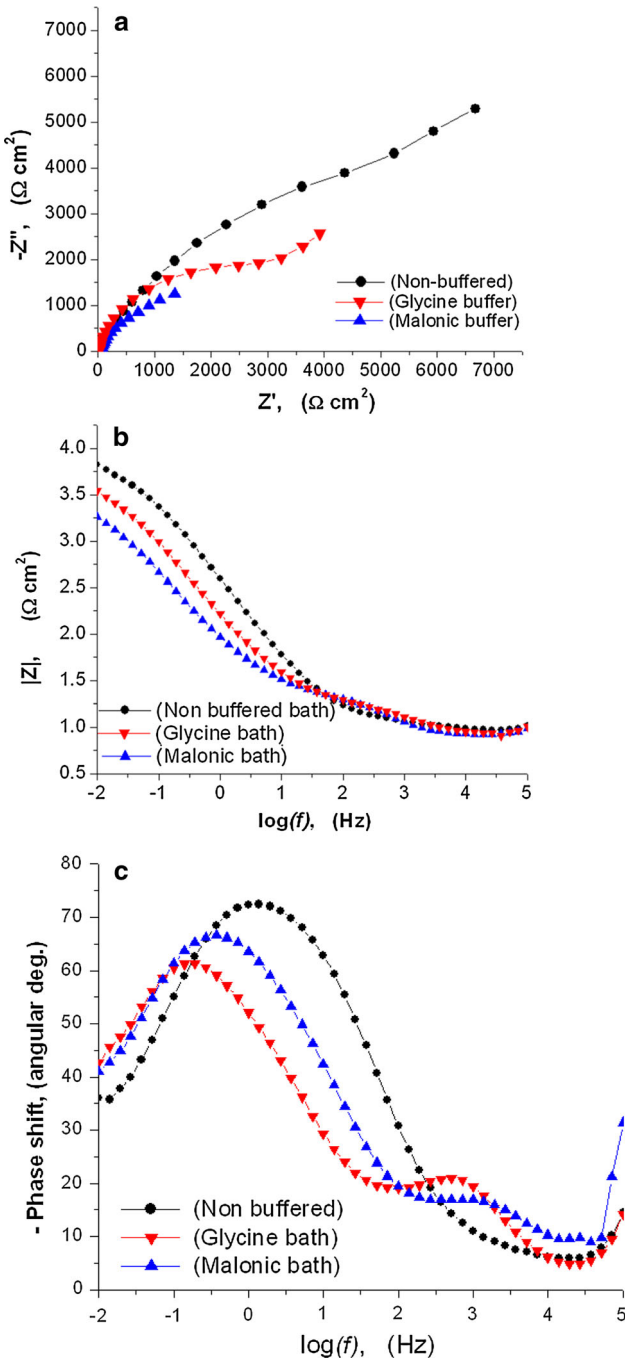

Fig. 8 Impedance spectra, in Nyquist (**a**) and Bode (**b**) plots of CeCC deposited in different baths on alkaline-etched AA2024 samples after 24 h of exposure to 3.5 % NaCl solution

3.4 Impedance measurements

The impedance measurements are performed to confirm the results obtained by the polarization measurements and to provide additional information about the corrosion durability of the Ce-conversion coatings and the processes at the interfaces in the metal/coating/electrolyte system.

Figures 7 and 8 show impedance spectra, in Nyquist and Bode plots, of CeCC deposited in different baths on mechanically polished (Fig. 7) and alkaline-etched (Fig. 8) specimens of AA2024 alloy after 24 h of exposure to the corrosion medium (3.5 % NaCl) used.

The curves in Figs. 7 and 8 show that the largest capacitive semi-circle refers to the coating obtained in a non-buffered bath, whereas the lowest one refers to that deposited in the presence of malonic acid. These results are in accord with the linear voltammetry data discussed above. A comparison of the impedance modules of the respective coatings at 10^{-2} Hz leads to the same conclusion, remarking the superior corrosion protective abilities of the coatings synthesized in glycine containing solutions, compared to the malonic ones. The coatings deposited in buffered baths have weaker barrier ability than those obtained in a non-buffered bath. Figures 7 and 8 feature two clear maxima in the function of the phase shift angle φ versus the frequency f in the Bode plots. The most pronounced maxima appear in $\varphi - \log(f)$ diagram for coatings deposited on alkaline-etched samples. Figure 8 shows that maxima appear at higher frequencies (in the range of about 10^{4}–10^{2} Hz), and at lower frequencies (in the range 10^{2}–10^{-2} Hz). In some cases, they are clearly separated from each other, whereas in other cases, they almost overlap. In accord with the conventional interpretation of the impedance spectra of coatings, the high frequency maximum and the high frequency time constant, respectively, are considered to be the response of the external layer of the coating and refers to the resistance and the capacitance of this layer. The lower frequency maximum is the response of the oxide layer and the corresponding charge transfer resistance R_{ct} of the metal/electrolyte interface, and the capacitance C_{edl} of the electric double layer on this interface. The presence of two maxima in φ versus $\log(f)$ dependence is an evidence that the CeCC obtained has a double-layered structure.

Different concepts are proposed for the mechanism of formation of two layers in CeCC. It is assumed that in case of CeCC deposited on AA6082 alloy, a conductive layer of Al-oxides/hydroxides is formed on the substrate surface in the course of the alkaline etching. This layer enables the proceeding of a Faraday reaction resulting in Ce-hydroxides precipitation on the cathodic zones. They are gradually substituting the conductive layer of Al-oxides/hydroxides [33]. This mechanism can be also accepted for the alkaline-etched AA2024 samples because of the chemical modification of their surface. However, it is inapplicable for the mechanically ground samples, where no such conductive layer of Al-oxides/hydroxides is formed. A different concept is advanced for AA2024 alloy [41]. It is assumed that the double layer structure of the CeCC is determined by the heterogeneous surface of this alloy containing

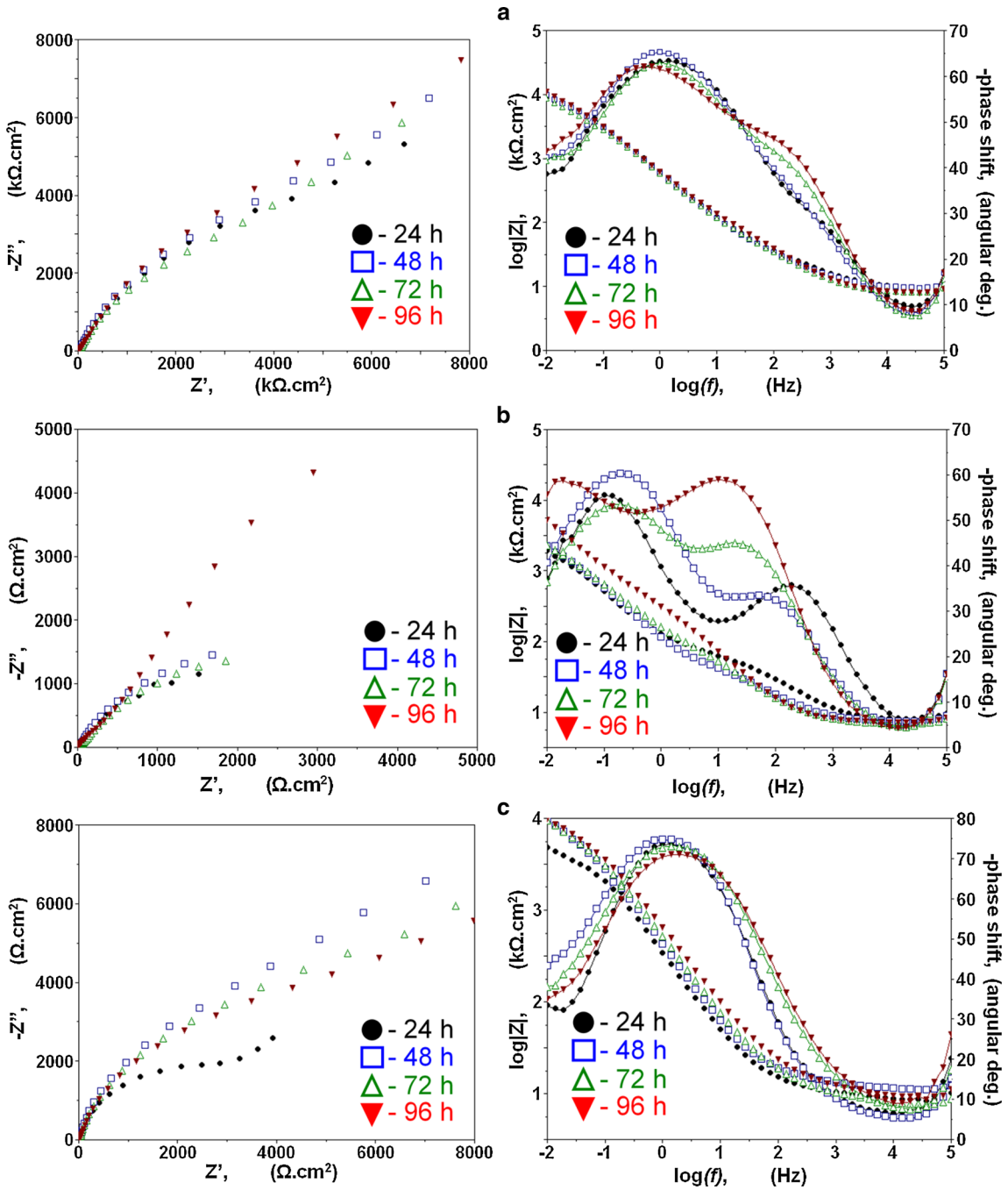

Fig. 9 Evolution of the impedance spectra of CeCC deposited in different baths on mechanically treated AA2024 samples during exposure to 3.5 % NaCl model corrosive medium. The deposition is carried out in a non-buffered bath (**a**); in a bath containing malonic acid (**b**) and in a bath containing glycine (**c**)

electrochemically active cathodic and anodic areas and Al-matrix. The different mechanism of CeCC deposition on these different sections of the surface predetermines the double- layer structure of the coating. However, some of the coatings obtained during the present research have a single-layer structure. Figure 7 shows that, in the case of CeCC deposition on mechanically ground samples in a glycine bath, a single maximum appears in the φ versus log(f) dependence. This indicates that these coatings are monolayered. The glycine buffer plays a key role in the course of CeCC deposition. Due to its reducing activity, glycine may remove CuO from the surface of re-deposited Cu on the alloy surface and thus activate these cathodic sections. Thus, the local reaction of CeCC deposition

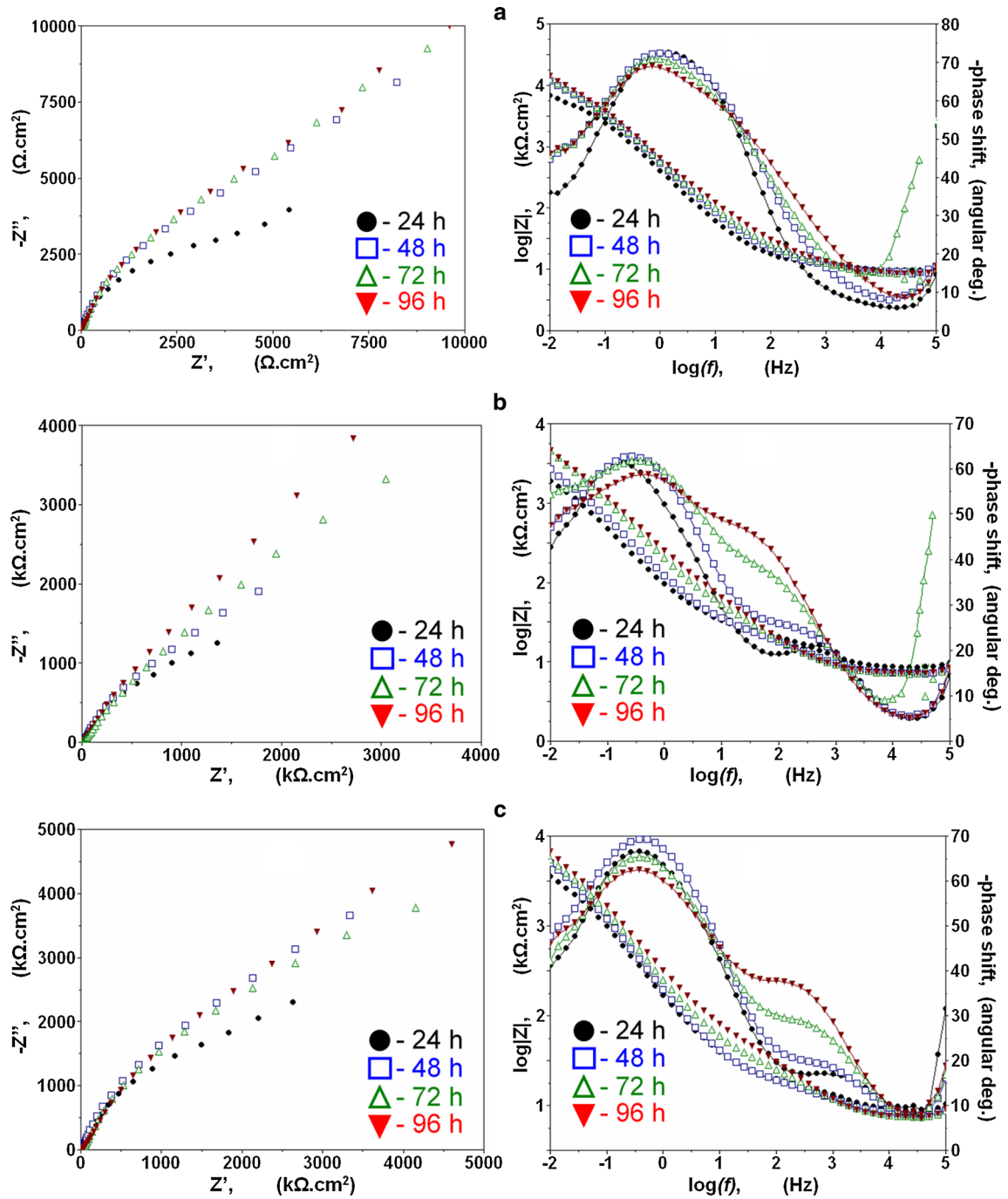

Fig. 10 Evolution of the impedance spectra of CeCC deposited in different baths on alkaline-etched AA2024 samples during exposure to 3.5 % NaCl model corrosive medium. The deposition is carried out in a non-buffered bath (**a**); in a bath containing malonic acid (**b**) and in a bath containing glycine (**c**)

becomes dominant. The Ce-oxide islands obtained spread over the entire surface in parallel with the formation of Al-oxides/hydroxides on the anodic areas. As a result, a single layer of an undefined mixture of Ce–Al oxide/hydroxides is formed. This model of island growth is proposed even in the earliest works dedicated to CeCC deposition [48].

The durability of the coatings against corrosion, related to the duration of exposure to corrosive medium until the first signs of corrosion, is estimated on the ground of the value of the impedance modulus at 10^{-2} Hz. It is found appropriate for comparative consideration despite its relative character. It is correlated to the polarization resistance

Table 4 Values of the impedance modulus $|Z|/k\Omega\ cm^{-2}$ and their evolution during the exposure of the respective samples to the 3.5 % NaCl corrosive medium

Bath	Pre-treatment	Time (h)			
		24	48	72	96
Non-buffered	Mechanical	8.51	9.66	8.83	10.81
	Alkaline	8.41	11.6	12.9	13.8
Malonic buffer	Mechanical	1.90	2.10	2.30	5.22
	Alkaline	1.85	2.59	4.78	4.51
Glycine buffer	Mechanical	3.69	5.59	9.66	9.72
	Alkaline	3.49	7.94	5.61	6.62

determined by the polarization measurements, but $|Z|$ is not identical to R_p.

The impedance spectra of CeCC deposited in different baths on mechanically ground samples after different exposure times are presented in Fig. 9, and the respective spectra for specimens, coated after alkaline etching, are represented in Fig. 10.

The data in Figs. 9 and 10 provide to determine the impedance modulus values $|Z|$ at 10^{-2} Hz for the respective specimens for different exposure times. The values obtained are summarized in Table 4.

It is evident from the data in Table 4 that the impedance modulus $|Z|$ for all CeCCs increases during the exposition to the corrosive medium. This increase of $|Z|$ resulting from the accumulation of corrosion products increases the barrier ability of the coatings. A more detailed examination of the impedance spectra shown in Figs. 8 and 9 and of φ versus $\log(f)$ relation, in particular, shows that the high frequency maximum for all coatings increases during the time of exposition. This increase is due to the increment of the exterior layer capacitive resistance as a result of the accumulation of corrosion products in the coating ruptures.

The data in Table 4 confirm the conclusions drawn from the polarization measurements. The highest impedance modulus and hence, the highest barrier ability, is measured for CeCC obtained in a non-buffered bath. The coatings deposited from a bath containing malonic acid have the lowest barrier ability. This difference originates from the CeCC thickness rather than from their structure and composition, as mentioned in Sect. 3.2.

4 Conclusions

The influence of two buffering additives, malonic acid and amino-acetic acid (glycine), on the deposition process and on the properties of the CeCC deposited on AA2024 alloy from H_2O_2-assisted $CeCl_3$ solutions is investigated. Complication and retention of the conversion process are observed because of two effects caused by the buffering additives: (1) deposition rate decreases because of the low pH value they sustain; (2) impeded oxidation of Ce(III) to Ce(IV) ions because of the buffering agents reducing activity. During CeCC deposition, an additional parameter plays an important role. This is the electrolyte loading, θ, outlining the relation between the volume of the bath V and the total surface area of the specimen S (i.e., $\theta = V/S$). At higher θ values ($\theta > 16$ cm), the deposition carried out in a bath containing malonic acid results in dark purple precipitates with a weak adherence to the substrate. Coatings of gold-yellow color typical for the CeCC are obtained after at least one or more depositions carried out in the same bath. These complications are not so notable in case of depositions using a bath containing glycine buffer.

The surface morphology and thickness of the coatings are considerably influenced by the presence of a buffer. Baths buffering leads to deposition of more uniform but thinner coatings that repeat the substrate surface.

Almost all coatings studied, except those obtained on ground substrates in a bath containing glycine buffer are double layered. The barrier ability of the coatings improves during their exposure to the corrosive medium, as a result of the increment of the capacitive resistance of the outer layer. It is caused by the deposition of corrosion products.

The coatings deposited in buffered baths do not show any signs of corrosion, despite their lower barrier ability, for up to 96 h of exposition.

All experimental results reported in this communication lead to the general conclusion that the idea to stabilize the conversion baths by introducing organic acids as buffering additives is not so promising after all.

Acknowledgments The authors gratefully acknowledge the financial support of project BG 051PO001-3.3.06-0038. We are thankful to Assoc. Prof. Dr. Eng. I. Nenov for the valuable information provided and for his assistance with the data interpretation. Dr. Gustavo Pelaez Lourido is acknowledged for the opportunity for international collaboration activities.

References

1. Starke EA, Staley JT (1996) Application of modern aluminum alloys to aircraft. Prog Aerosp Sci 32:131–172
2. Tottem GE, Meckenzie DS (2003) Handbook of aluminium. Marcel Dekker, NY
3. Foley RT (1986) Localized corrosion of aluminum alloys-a review. Corros Sci 42:277–288
4. Guillaumin V, Mnankovski G (1999) Localized corrosion of 2024 T351 aluminium alloy in chloride media. Corros Sci 41:421–438
5. Fonseca ITE, Lima N, Rodriguez JA, Perreira MIS (2002) Passivity breakldown of Al 2024–T3 alloy in chloride solutions: a test of the point defect model. Electrochem Commun 4:252–357
6. Groshart EA (1984) Design and finish requirements of high strength steels. Met Finish 82:69–70

7. Kending MW, Davenport AJ, Issacs HS (1993) The mechanism of corrosion inhibition by chromate conversion coatings from X-ray absorption near edge spectroscopy (Xanes). Corros Sci 34:41–49
8. Fahrenholz WG, O'Keefe MY, Zhou H, Grant JT (2002) Characterization of cerium-based conversion coatings for corrosion protection of aluminum alloys. Sufr Coat Technol 155:208–213
9. EU Directive 2002/95/EC. Restriction of Hazardous Substances in Electrical and Electronic Equipment. (RoHS directive 2002), www.broadcom.com/docs/, www.chem.agilent.com/
10. U.S. Department of Health and Human Services, Public Health Service, Agency of Toxic Substances and Disease Registry (2008) Toxicological profile for Chromium, www.atsdr.cdc.gov/toxprofiles/tp7.pdf
11. U.S. Environmental Protection Agency Washington, DC, August (1998) Toxicological review of hexavalent chromium. http://www.epa.gov/iris/toxreviews/0144tr.pdf
12. Falconnet PJ (1993) The rare earth industry: a world of rapid change. J Alloys Comp 192:114–117
13. Muecke G, Möller P (1988) The not-so-rare earths. Sci Am 258:72–77
14. Hinton BRW, Arnott DR, Ryan E (1984) The inhibition of aluminum corrosion by cerium cations. Metals Forum 7:211–217
15. Hinton BRW, Ryan E, Arnott DR, Thrathen PN, Willson L, Williams BE (1985) The inhibition of aluminium alloy corrosion by rare earth metal cations. Corros Austral 10:12–17
16. Hinton BRW, Arnott DR, Ryan E (1986) Matter Forum 9:162
17. Hinton B, Huges A, Taylor R, Handerson M, Nelson K, Wilson L, Proceedings of the 13th international corrosion conference Melburne, (Australia)
18. Hamdy AS, Beccaria AM (2005) Effect of surface preparation prior to cerium pre-treatment on the corrosion protection performance of aluminum composites. J Appl Electrochem 35:473–478
19. Yasakau KA, Zheludkevich ML, Ferreira MGS (2008) Lanthanide salts as corrosion inhibitors for AA5083. Mechanism and efficiency of corrosion inhibition. J Electrochem Soc 155:C169–C177
20. Machkova M, Matter EA, Kozhukharov S, Kozhukharov V (2013) Effect of the anionic part of various Ce(III) salts on the corrosion inhibition efficiency of AA2024 aluminium alloy. Corr Sci 69:396–405
21. Arenas MA, Bethencourt M, Botana FJ, de Damborenea J, Marcos M (2001) Inhibition of 5083 aluminium alloy and galvanised steel by lanthanide salts. Corros Sci 43:157–170
22. Dias SAS, Marques A, Lamaka SV, Simões A, Diamantino TC, Ferreira MGS (2013) Unravelling the corrosion inhibition mechanisms of bi-functional inhibitors by EIS and SEM–EDS. Electrochim Acta 112:549–556
23. Matter EA, Kozhukharov S, Machkova M, Kozhukharov V (2013) Electrochemical studies on the corrosion inhibition of AA2024 aluminium alloy by rare earth ammonium nitrates in 3.5 % NaCl solutions. Mater Corros 64(5):404–408. doi:10.1002/maco.201106349
24. Tamborim SM, Maisonnave APZ, Azambuja DS, Englert GE (2008) An electrochemical and superficial assessment of the corrosion behavior of AA 2024-T3 treated with metacryloxypropylmethoxysilane and cerium nitrate. Surf Coat Technol 202:5991–6001
25. Tavandashti NP, Sanjabi S (2010) Corrosion study of hybrid sol–gel coatings containing boehmite nanoparticles loaded with cerium nitrate corrosion inhibitor. Prog Org Coat 69:384–391
26. Kozhukharov S, Kozhukharov V, Schem M, Aslan M, Wittmar M, Wittmar A, Veith M (2012) Protective ability of hybrid nanocomposite coatings with cerium sulphate as inhibitor against corrosion of AA2024 aluminium alloy. Prog Org Coat 73:95–103
27. Cabral AM, Trabelsi W, Serra R, Montemor MF, Zheludkevich ML, Ferreira MGS (2006) The corrosion resistance of hot dip galvanised steel and AA2024-T3 pre-treated with bis-[triethoxysilylpropyl] tetrasulfide solutions doped with $Ce(NO_3)_3$. Corros Sci 48:3740–3758
28. Lee YL, Cheen FJ, Lin CS (2013) Corrosion resistance studies of cerium conversion coatings with fluoride-free pretreatment on AZ91D magnesium alloy. J Electrochem Soc 160:C28–C35
29. Rivera BF, Johnson BY, O'Keefe M, Farenholz WG (2004) Deposition and characterization of cerium oxide conversion coatings on aluminum alloy 7075-T6. Surf Coat Technol 176:349–356
30. O'Keefe M. J., Geng S., Joshi, S (2007) Cerium-based conversion coatings as alternatives to hex chrome. Metalfinishing 105:25–28
31. Fahrenholtz WG, O'Keefe MJ, Zhou H, Grant JT (2002) Characterization of cerium-based conversion coatings for corrosion protection of aluminum alloys. Surf Coat Technol 155:208–213
32. Palomino LEM, Aoki IV, de Melo HG (2006) Microstructural and electrochemical characterization of Ce conversion layers formed on Al alloy 2024-T3 covered with Cu-rich smut. Electrochim Acta 51:5943–5953
33. Dekroly A, Petitjean J-P (2005) Study of the deposition of cerium oxide by conversion on to aluminium alloys. Surf Coat Technol 194:1–9. doi:10.1016/j.surfcoat.2004.05.012
34. Huges AE, Scholes FH, Glenn AM, Lau D, Muster TH, Hardin SG (2009) Factors influencing the deposition of Ce-based conversion coatings, part I: the role of Al^{3+} ions. Surf Coat Technol 203:2927–2936
35. Aramaki K (2006) The effect of modification with hydrogen peroxide on a hydrated cerium(III) oxide layer for protection of zinc against corrosion in 0.5 M NaCl. Corros Sci 48:766–782
36. Pinc W, Geng S, O'Keefe M, Fahrenholtz W, O'Keefe T (2009) Effects of acid and alkaline based surface preparations on spray de posited cerium based conversion coatings on Al2024-T3. Appl Surf Sci 255:4061–4065
37. Zhao D, Sun J, Zhang L, Tan Y, Li J (2010) Corrosion behavior of rare earth cerium based conversion coating on aluminum alloy. J Rare Earths 28:371–374
38. Aziz I, Qi Z, Min X (2009) Corrosion inhibition of SiCp/5A06 aluminum metal matrix composite by cerium conversion treatment. Chin J Aeronaut 22:670–676
39. Lourier YY (1967) Manual on analytical chemistry. Gov. Ed. "Chemistry", Moscow, pp 305–307
40. Damaskin BB, Petriy OA (1983) Introduction in the electrochemical kinetics. Gov. Ed. Superior School, Moscow, p 52
41. Scholes FH, Soste C, Hughes AE, Hardin SG, Curtis PR (2006) The role of hydrogen peroxide in the deposition of cerium-based conversion coatings. Appl Surf Sci 253:1770–1780
42. Newmann B, Steinbock O, Muller SC, Dalal NS (1997) Stoichiometric fingerprinting as an aid in understanding complex reactions: the oxidation of malonic acid by Cerium(IV). J Phys Chem A 101:2743–2745
43. Santos E, Hindelang P, Quaino P, Schmickler W (2011) A model for the Heyrovsky reaction as the second step in hydrogen evolution. Phys Chem Chem Phys 13:6992–7000
44. Osadchaya LI, Sokolov VV, Trushnikova L, Zubareva AP (2003) Preparation of cerium hydrides. Inorg Mater 39:1142–1143
45. Yasakau KA, Zheludkevich ML, Lamaka SV, Ferreira MGS (2006) Mechanism of corrosion inhibition of AA2024 by rare-earth compounds. J Phys Chem B 110:5515–5528
46. Matter EA, Kozhukharov SV, Machkova MS (2011) Effect of preliminary treatment on the superficial morphology and the corrosion behaviour of AA2024 aluminum alloy. Bul Chem Commun 43:23–30

47. Matter E, Kozhukharov S (2010) Correlation between preliminary pretreatments and the behaviour of AA2024 aluminium alloy in 3.5 % NaCl model corrosive medium. Ann Proc Univ Rousse (Bulgaria) 49:14–19

48. Arnott DR, Ryan NE, Hinton BRW, Sexton BA, Hughes AE (1985) Auger and XPS studies of cerium corrosion inhibition on 7075 aluminum alloy. Appl Surf Sci 22–23:236–251